Consequences of large θ_{13} for the turbulence signatures in supernova neutrinos

James P. Kneller and Alex W. Mauney

Phys. Rev. D **88**, 025004 — Published 1 July 2013

DOI: 10.1103/PhysRevD.88.025004

The consequences of large θ_{13} for the turbulence signatures in supernova neutrinos

James P. Kneller* and Alex W. Mauney†
Department of Physics, North Carolina State University, Raleigh, North Carolina 27695, USA

The set of transition probabilities for a single neutrino emitted from a point proto-neutron source after passage through a turbulent supernova density profile have been found to be random variates drawn from parent distributions whose properties depend upon the stage of the explosion, the neutrino energy and mixing parameters, the observed channel, and the properties of the turbulence such as the amplitude $C_\star$. In this paper we examine the consequences of the recently measured mixing angle θ_{13} upon the neutrino flavor transformation in supernova when passing through turbulence, in order to provide some clarity as to what one should expect in the way of turbulence effects in the next supernova neutrino burst signal. We find the measurements of a relatively large value of θ_{13} means the neutrinos are relatively immune to small, $C_\star \lesssim 1\%$, amplitude turbulence but as $C_\star$ increases the turbulence effects grow rapidly and spread to all mixing channels. For $C_\star \gtrsim 10\%$ the turbulence effects in the high (H) density resonance mixing channels are independent of θ_{13} but non-resonant mixing channels are more sensitive to turbulence when θ_{13} is large.

PACS numbers: 47.27.-i,14.60.Pq,97.60.Bw

I. INTRODUCTION

The progress in the field of supernova neutrinos over the past decade has been frenetic. The rich phenomenology of neutrino collective effects [1–15] (for a review see [16, 17]) have received the most attention but there has been an equally radical overhaul of the Mikheyev, Smirnov & Wolfenstein (MSW) [18, 19] effect as applied to supernovae ever since it was realized by Schirato & Fuller [20] that the shockwave racing through the stellar mantle could leave an imprint upon the neutrinos emitted from the cooling proto-neutron star [20–26]. Recent studies indicate Earth matter effects may be minimal [27]. From this ever-growing body of literature one now expects that the neutrino signal from the next supernova in our Galaxy will be pregnant with information. If the signal can be decoded we might be able to both determine any unresolved properties of the neutrino and also to observe the explosion while it is still deep within the star. Yet most, though not all, of these studies of neutrino propagation in supernovae use spherically symmetric density profiles either in a parametrized form or taken from one-dimensional hydrodynamical simulations. While the use of one-dimensional hydrodynamical profiles for neutrino signal construction is probably adequate for certain situations - such as neutrinos from Oxygen, Neon, Magnesium supernova [28–30] which explode in spherically symmetric simulations [31–33] - it is now apparent that iron core collapse supernova should not be expected to be spherically symmetric. Large scale inhomogeneities are created deep within the explosion and one observes turbulence during the neutrino heating/Standing Accretion Shock Instability phase [41–48] leading to the expectation of violent fluid motions and turbulence in the stellar mantle after the shock is revived and moves outwards. Like collective and shock effects, turbulence is another supernova feature that can leave its fingerprints upon the neutrino burst [10, 49–52]. At first glance turbulence is just a case of a more complicated MSW effect but, upon further reflection, one realizes that the randomness of the profiles means the transition probabilities for a particular neutrino - the set of probabilities that relates the initial state to the state after passing through the supernova - along a given ray are not unique: they will depend upon the exact turbulence pattern seen by the neutrino as it traveled through the supernova. The transition probabilities are drawn from a distribution whose properties will depend upon the stage of the explosion, the character of the turbulence, and the neutrino energy and mixing parameters, including θ_{13}. When the mixing angle θ_{13} was unknown it was difficult to make robust statements about the effect of turbulence because at one value of θ_{13} the turbulence effects would be negligible, at another the turbulence would be endemic. The recent measurements of the last mixing angle θ_{13} by T2K [34], Double Chooz [37], RENO [35] and Daya Bay [36] are all in the region of $\theta_{13} \approx 9°$, significantly higher than the Dighe & Smirnov [38] threshold, and it is now possible to be more definitive about the consequences of turbulence.

A focused consideration of turbulence effects upon supernova neutrinos for values of θ_{13} as large as 9° is presently not available and it is the purpose of this paper to fill in that hole in the literature. Our calculations follow on from the work of Kneller & Volpe [52] upon which we shall rely heavily for the techniques used to calculate the turbulence effects and as reference for our results. We first describe the calculations we undertook then present our results for the turbulence effects when the turbulence amplitude is small, less than 1% comparing large and small θ_{13} in order to demonstrate why values of $\theta_{13} \approx 9°$ greatly reduce the sensitivity of the neutrinos to small amplitude turbulence. We then turn

* jpknelle@ncsu.edu
† awmauney@ncsu.edu

to the case of large amplitude turbulence and compute the expectation values of the transition probability distributions in both neutrinos and antineutrinos again comparing large and small θ_{13} in order to show why, in this scenario, large θ_{13} *does not* change the sensitivity of the neutrinos to the turbulence. We finish with a summary and our conclusions.

II. DESCRIPTION OF THE CALCULATIONS

The quantities we are interested in calculating are the probabilities that some initial neutrino state $|\nu(x)\rangle$ at x is later detected as the state $|\nu(x')\rangle$ at x'. These probabilities are computed from the S-matrix which relates the initial and final states via $|\nu(x')\rangle = S(x', x)\,|\nu(x)\rangle$. The S-matrix is found by solving the equation

$$\imath \frac{dS}{dx} = H\,S \tag{1}$$

where H is the Hamiltonian. In matter the Hamiltonian is composed of at least two terms: the vacuum contribution H_0 and the MSW potential V. When solving for S one must work in a particular basis and the basis determines the structure of the terms in the Hamiltonian. In the 'mass' basis the vacuum Hamiltonian is diagonal and described by two mass squared differences $\delta m^2_{ij} = m^2_i - m^2_j$ and the neutrino energy E. Through this paper we shall use the values of $\delta m^2_{21} = 8 \times 10^{-5}$ eV^2 and $|\delta m^2_{32}| = 3 \times 10^{-3}$ eV^2 which are consistent with present experimental values. In the flavor basis the off-diagonal elements are non-zero leading to the phenomenon of flavor oscillations. The two bases are related by the Maki-Nakagawa-Sakata-Pontecorvo [39, 40] unitary matrix parametrized by three mixing angles, θ_{12}, θ_{13} and θ_{23}, a CP phase and two Majoranna phases. For this paper we adopt $\sin^2 2\theta_{12} = 0.83$ and $\sin^2 2\theta_{23} = 1$ which are, again, consistent with present experimental values

In contrast, the matter potential is diagonal in the flavor basis because the matter picks out the neutrino flavors. The common neutral current contribution to the matter potential may be dropped because it leads only to a global phase which is unobservable leaving just the charged current potential, $\sqrt{2} G_F n_e(r)$ where G_F is the Fermi constant and $n_e(r)$ the electron density, which affects just the electron neutrino/antineutrino i.e. the element V_{ee}. In addition to the matter potential, it has been found that the neutrino density in supernovae is so high that an additional potential due to neutrino self-interactions must be included. This neutrino self-coupling has been shown to lead to very interesting behavior but for our purposes the self-interaction is negligible when the turbulent region in the star has moved beyond 1000 km so we shall ignore this contribution.

When the vacuum and matter terms are added together the Hamiltonian is neither diagonal in the mass nor the flavor bases so one would expect oscillations of both the flavor and mass probabilities. These oscillations are a source of potential confusion for any analysis. A basis can be found which diagonalizes H for a given value of the electron density in the sense that there is a matrix U such that $U^\dagger H U = K$ where K is the diagonal matrix of eigenvalues. This basis is known as the matter basis which becomes the mass basis (up to arbitrary phases) when the matter potential disappears. The matter mixing matrix U which achieves this diagonalization depends upon the position through the star therefore $dU/dx \neq 0$ in general. The non-zero derivative of the matter mixing matrix re-introduces off-diagonal elements into the matter basis Hamiltonian which will lead to mixing between the matter basis states if they become large. We refer the reader to Kneller & McLaughlin [55] and Galais, Kneller & Volpe [12] for a more detailed description of the matter mixing matrix. We shall report our results using the matter basis states throughout this paper.

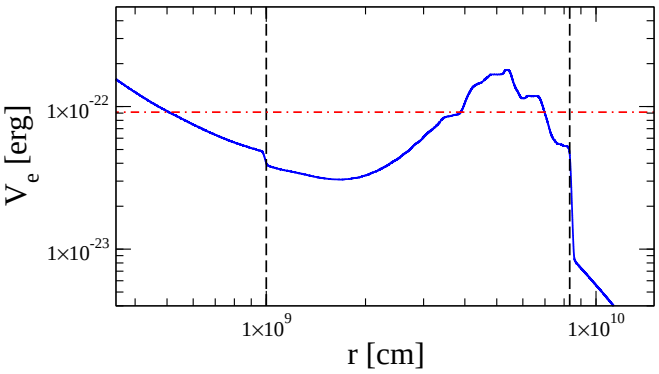

FIG. 1. The matter potential as a function of distance through a supernova taken from a hydrodynamical simulation at 4.5 s post bounce. The vertical lines indicate the positions of the reverse and forward shock in the profile. The horizontal dashed-dotted line is the two-flavor resonance density for a 25 MeV neutrino with mixing angle $\sin^2 2\theta = 0.1$ and mass splitting $\delta m^2 = 3 \times 10^{-3}$ eV^2 i.e. the high (H) density resonance

Next we must introduce the turbulent density profile though which the neutrinos will propagate. Ideally one would like to use density profiles taken from multi-dimensional simulations but at the present time that is not possible. The current multi-dimensional simulations do not extend out to the region of $r \gtrsim 10^4$ km where the turbulence would have its greatest effects because the matter there has little bearing upon the explosion, and even if they did, they do not run to sufficiently late post-bounce times to see the shock move out there. Finally, the dynamic scale the simulations would need to cover would be of order forty to fifty decibels - four to five orders of magnitude - because the neutrino oscillation wavelength is significantly smaller than the radius in the high (H) density resonance region and beyond. For these reasons the effect of the turbulence upon the neutrinos is most often modeled as a random field. We adopt a one-dimensional supernova profile from a hydro-

dynamical simulation and in order to facilitate comparison the profile we select is the same 4.5 s post bounce snapshot taken from Kneller, McLaughlin & Brockman used in Kneller & Volpe. This profile is shown in figure (1). In the figure we find two shocks: the forward shock at r_s formed from the core bounce, and the reverse shock at r_r formed by the wind created above the proto-neutron star running into the material ahead of it. In multi-dimensional simulations of supernova both these shock fronts are distorted leading to strong turbulence in the region between them. The reason we select the profile shown in figure (1) is because the shock in this simulation has propagated out to the H resonance region at this time. Simulations of supernova using different progenitor structures have found considerable variation in the delay before the shock arrives in the H resonance region, see Lund & Kneller [57].

Now that we have our profile we need to adopt a neutrino energy. The effect of turbulence upon a given neutrino at a given epoch depends upon its energy because different neutrino energies have different resonance densities and the turbulence will not affect these resonances equally. This is shown in Galais *et al.* [56] where the reader may find a plot of the effect of a single realization of turbulence inserted into exactly the same density profile we will use upon a neutrino spectrum albeit at a mixing angle of $\theta_{13} = 0.573°$. For this paper we shall use a neutrino energy such that the H resonance density does not intersect the shocks. The reason we avoid the shocks is twofold. Hydrodynamical simulations typically yield 'soft' shocks that do not cause transitions between the neutrino states if the mixing angle is too big [20, 23, 56, 57]. This lack of a transition is unphysical. The second reason is that we wish to focus solely upon the turbulence effect and diabatic[1] MSW transitions caused by the shocks complicates the interpretation. For these reasons we focus upon neutrino energies in the range $20 - 30$ MeV and the two-flavor resonance density for a 25 MeV is shown in figure (1). The reader can verify that it does not intersect the profile at either shock.

For future reference we shown in figure (2) the transition probability P_{23} for a normal hierarchy and $\bar{P}_{13}$ for an inverted hierarchy using the density profile shown in figure (1) for a 25 MeV neutrino as a function of the mixing angle θ_{13}. Note that these transition probabilities are very close to zero when using a mixing angle given by $\sin^2 2\theta_{13} = 0.1$. The reader may be surprised to see that the figure indicates the transition probabilities change from the diabatic limit, $\bar{P}_{13} = 1$ or $P_{23} = 1$, to the adiabatic limit $\bar{P}_{13} = 0$ or $P_{23} = 0$ is not monotonic in the H resonance channel because of the aforementioned presence of the multiple H resonances in the profile. The multiple H resonances leads to an interference effect which is sensitive to θ_{13} when $0.1° \lesssim \theta_{13} \lesssim 1°$ for this neutrino energy, profile and mass splitting [53, 54].

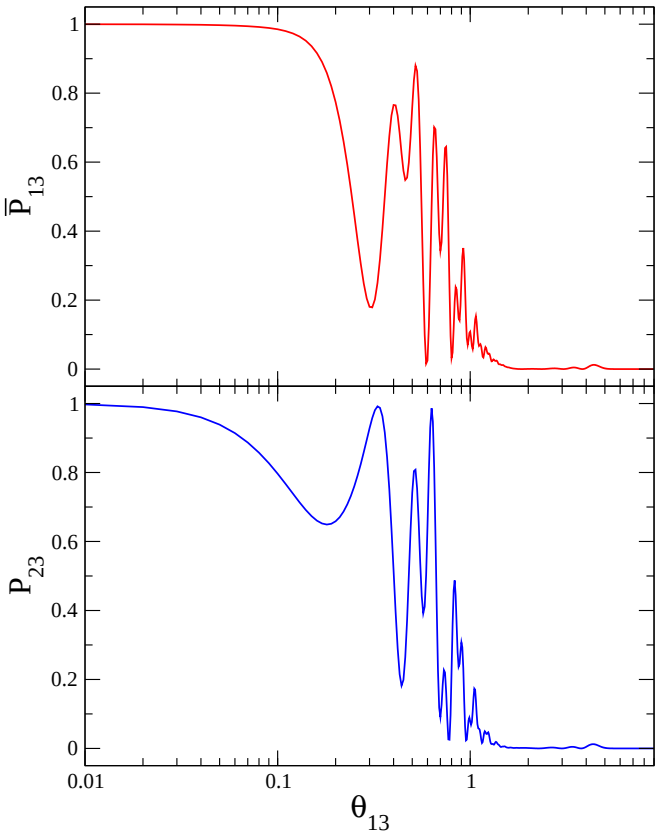

FIG. 2. The transition probability $\bar{P}_{13}$ in an inverted hierarchy (top panel) and P_{23} in a normal hierarchy (lower panel) after passing through the density profile shown in figure (1) for a 25 MeV neutrino as a function of the mixing angle θ_{13}

A. Modeling the turbulence

The turbulence is introduced by multiplying the profile in the region between the reverse and forward shocks by a factor $1 + F(r)$ where $F(r)$ is a Gaussian random field with zero mean. An example a turbulent profile generated this way can be seen in figure (1) of Kneller & Volpe. Since the quality of our results in this entire paper rests upon our ability to do this well, it is worth our effort to explain carefully how $F(r)$ was constructed. The random field is represented using a Fourier series i.e.

$$F(r) = C_\star \tanh\left(\frac{r - r_r}{\lambda}\right) \tanh\left(\frac{r_s - r}{\lambda}\right) \times \sum_{n=1}^{N_k} \sqrt{V_n}\left\{A_n \cos(k_n r) + B_n \sin(k_n r)\right\}. \quad (2)$$

for radii between $r_r \leq r \leq r_s$ and zero outside this range. The two radii r_r and r_s are the positions of the reverse

[1] Throughout this paper we shall use the term 'diabatic' to mean the opposite of 'adiabatic': the reader will sometimes encounter in other literature the term 'non-adiabatic' instead.

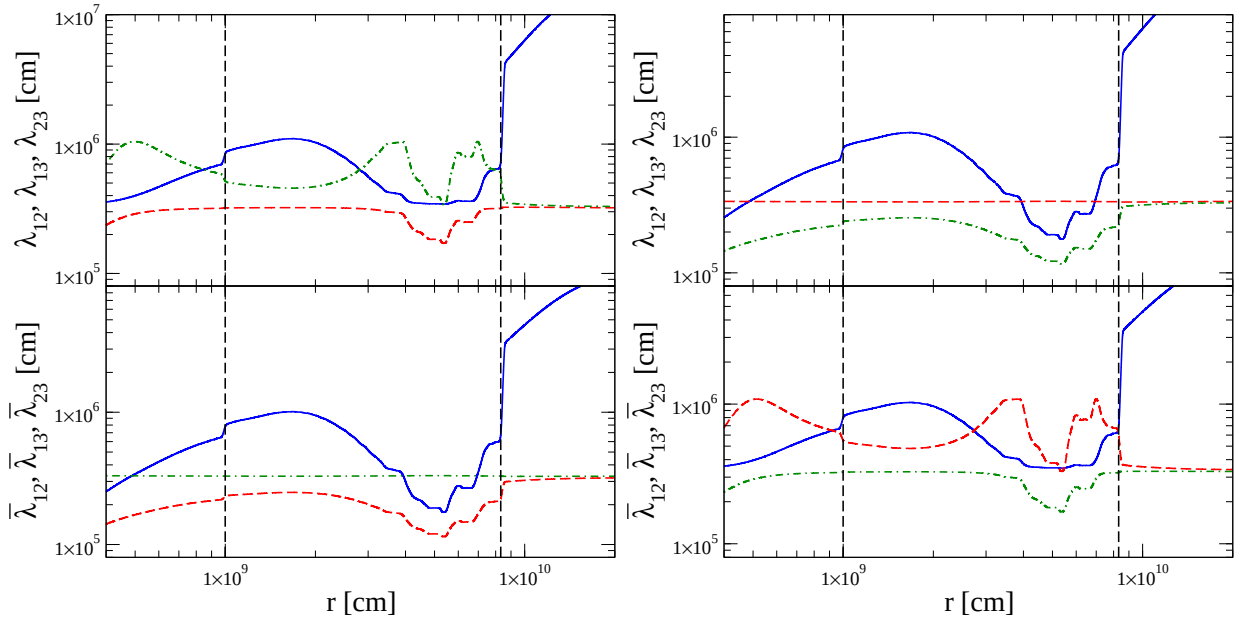

FIG. 3. The reduced wavelength of the splitting between the eigenvalues. The density profile is that shown in figure (1), the neutrino energy is 25 MeV and the neutrino mixing angle θ_{13} is given by $\sin^2 2\theta_{13} = 0.1$. In the left panel we show the normal hierarchy case, in the right panel the inverted and the top row of each is for the neutrinos and the bottom row for antineutrinos.

and forward shock respectively found in the underlying profile. In this equation the parameter $C_\star$ sets the amplitude of the fluctuations. The two tanh terms are included to suppress fluctuations close to the shocks and prevent discontinuities at r_s and r_r, and the parameter λ is a scale over which the fluctuations reach their extent size. We set $\lambda = 100$ km. In the second half of equation (2) the members of the set of co-efficients $\{A\}$ and $\{B\}$ are independent standard Gaussian random variates with zero mean thus ensuring the vanishing expectation value of F. The N_k wavenumbers form a set $\{k\}$ and, finally, the parameters V_n are k-space volume co-efficients to which we return shortly. The power spectrum of the random field was selected to be

$$E(k) = \frac{(\alpha - 1)}{2\, k_\star} \left(\frac{k_\star}{|k|} \right)^\alpha \Theta(|k| - k_\star). \qquad (3)$$

Here $k_\star$ is the cutoff scale, α is the spectral index and Θ is the Heaviside step function. Throughout this paper we shall use a wavenumber cutoff $k_\star$ set to $k_\star = \pi/(r_s - r_r)$ i.e. a wavelength twice the distance between the shocks and we shall adopt the Kolmogorov spectrum where $\alpha = 5/3$. The method of fixing the N_k k's, V's, A's and B's for a realization of F is 'variant C' of the Randomization Method described in Kramer, Kurbanmuradov, & Sabelfeld [59]. This Randomization Method partitions the k-space into N_k regions and from each we select a random wavevector using the power-spectrum, $E(k)$, as a probability distribution. The volume parameters V_n are the integrals of the power spectrum over each partition if the power spectrum is normalized to unity. Variant C of the Randomization Method divides the k-space so that the number of partitions per decade is uniform over N_d decades starting from a cutoff scale $k_\star$. The logarithmic distribution of the modes is designed to ensure the quality of the agreement between the exact statistical behavior of the field and that of an ensemble of realizations is uniform over a the range of lengthscales considered i.e. it is scale invariant. This feature is important for our study because the oscillation wavelength of the neutrinos is constantly changing as the density evolves. The evolution of the reduced oscillation wavelengths for the neutrinos - $\lambda_{ij} = 1/|\delta k_{ij}|$ - and antineutrinos - $\bar{\lambda}_{ij} = 1/|\delta \bar{k}_{ij}|$ - where δk_{ij} and $\delta \bar{k}_{ij}$ are the differences between the eigenvalues i and j of the neutrinos and antineutrinos respectively - as a function of distance through the profile are shown in figure (3) for both a normal and an inverse hierarchy when the mixing angle θ_{13} is set to $\sin^2 2\theta_{13} = 0.1$ and the energy is $E = 25$ MeV. Again the reverse and forward shocks are indicated by the two vertical dashed lines. This figure can be used to determine a suitable value for N_d because we observe that in the region between the shocks the typical wavelengths are $\gtrsim 1$ km which is the minimum lengthscale we need to cover [51, 60]. This is approximately 4 orders of magnitude smaller than the turbulence cut-off scale $1/k_\star$ thus we deduce that we need to pick $N_d \geq 4$ to cover the necessary decades in k-space.

With N_d determined we now seek a suitable value of N_k by requiring that the statistical properties of an ensemble of random field realizations closely match the exact properties for the field. The statistical property we compute is the second order structure function $G_2(\delta r)$, the expectation value of the square difference between

the field at two radial points, and given by

$$G_2(\delta r) = \langle [F(r+\delta r) - F(r)]^2 \rangle \tag{4}$$

where δr is the separation. The function $G_2(\delta r)$ is related to the two-point correlation function $B(\delta r)$ via $G_2(\delta r)/2 = 1 - B(\delta r)$ and, for the power spectrum we have adopted, we can compute the two-point correlation function analytically to be

$$B(\delta r) = \frac{(\alpha-1)}{2}\,(2\pi\, k_\star\, \delta r)^{\alpha-1}\left\{\exp\left(\frac{\imath\pi\alpha}{2}\right)\,\Gamma(1-\alpha, 2\imath\pi\, k_\star\, \delta r) + \exp\left(\frac{\imath\pi\alpha}{2}\right)\,\Gamma(1-\alpha, -2\imath\pi\, k_\star\, \delta r)\right\}. \tag{5}$$

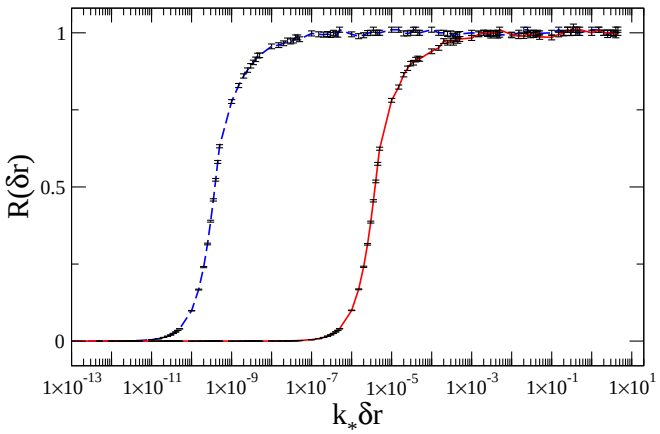

FIG. 4. The ratio $R(\delta r)$ of the numerically calculated structure function to the analytic result as a function of $k_\star \delta r$. The two curves in the figure correspond to $\{N_k, N_d\} = \{50, 5\}$ (red solid) and $\{N_k, N_d\} = \{90, 9\}$ (blue dashed). At every $k_\star \delta r$ we generated 30,000 realization of the field and the error bar on each point is the standard deviation of the mean.

where $\Gamma(n, x)$ is the upper incomplete Gamma function. In figure (4) we show the ratio $R(\delta r)$ of the numerically calculated structure function to the exact solution as a function of the scale $k_\star \delta r$ when we use either $N_k = 50$ wavenumbers spread over $N_d = 5$ decades or $N_k = 90$ wavenumbers over $N_d = 9$ decades. The numerical calculation is the average of 30,000 realizations of the turbulence and the error bar on each point is the standard deviation of the sample mean. The figure indicates that the method we use to generate random field realizations reproduces the analytic results for the structure function very well and with high efficiency because good agreement between the statistics of the ensemble and the exact result requires just $N_k/N_d = 10$. In fact, like Kramer, Kurbanmuradov, & Sabelfeld [59] before us, we find even N_k/N_d ratios of just $N_k/N_d \sim 2-3$ are sufficient to give acceptable agreement. We re-assure the reader we shall stick with $N_k/N_d = 10$.

III. RESULTS

With the construction of the random fields in place we can proceed to generate a turbulent profile and propagate neutrinos and antineutrinos through it. This construction and propagation recipe is then repeated a minimum of one thousand times - sometimes much larger - to construct an ensemble of transition probabilities of size N. Once we have our sample we can then go ahead and compute means $\langle P_{ij} \rangle$, variances σ_{ij}, etc. The hierarchy will be set to normal and we shall comment on how our results translate to the inverted hierarchy. The neutrino energy will be specified when necessary. The turbulence effects - or lack of them - when using a value of θ_{13} close to the present measurements was not fully explored in previous studies so to make a connection with previous works, and to explain why a large value of θ_{13} gives the results that it does, we shall consider multiple values of θ_{13} in order to show what other possibilities would have produced in contrast.

A. Small amplitude turbulence

For small amplitude turbulence only the H resonant channel is affected: mixing between states ν_2 and ν_3 for a normal hierarchy and states $\bar{\nu}_1$ and $\bar{\nu}_3$ for an inverted. Previously it has been found that effects could appear in the neutrinos even for turbulence amplitudes in the range $10^{-5} \lesssim C_\star \lesssim 0.1$ when the mixing angle was set at $\sin^2 2\theta_{13} = 4 \times 10^{-4}$. If we allow the value of θ_{13} to float then we find the normal hierarchy H resonance channel transition probability P_{23} can become more or less diabatic. This can be explained from the behavior of the diabaticity parameter Γ_{23} [55], which characterizes the degree of mixing in the H resonance channel for a normal hierarchy. This quantity is inversely proportional to the difference δk_{23} between the eigenvalues k_2 and k_3 and proportional to the derivative of the matter mixing angle $\tilde{\theta}_{13}$. Increasing θ_{13} increases the eigenvalue splitting and also makes the resonance 'wider' in the sense that the change between the limiting values of the matter mixing angle $\tilde{\theta}_{13}$ occurs over a greater extent reducing the matter angle derivative. Both effects decrease the diabaticity and, for these reasons, reaching the depolarization limit for P_{23} becomes more difficult if the domain of turbulence

is fixed as is the case here. If the profile were changed so as to allow a larger turbulence region then eventually one should expect to reach the depolarization limit no matter what the mixing angle. A similar argument applies when θ_{13} becomes small: now the diabaticity increases as θ_{13} decreases because the splitting between the eigenvalues at the resonance decreases and the transition occurs more rapidly. Either way, as θ_{13} varies the distributions for the transition probability P_{23} will differ from the uniform distributions seen in Kneller & Volpe leading to subsequent evolution of the expectation values and distribution variances. This evolution with θ_{13} is seen in figure (5) where we plot the mean value $\langle P_{23}\rangle$ and the standard deviation of the samples from a single emission point as a function of θ_{13} for three neutrino energies. The reader should compare the evolution of $\langle P_{23}\rangle$ in this figure with that in figure (2). For all three energies, the mean value of $\langle P_{23}\rangle$ has an inflection region between $0.1^\circ \lesssim \theta_{13} \lesssim 1^\circ$: for the smaller values of θ_{13} we see $\langle P_{23}\rangle > 1/2$, for the larger $\langle P_{23}\rangle < 1/2$ and for $\theta_{13} \sim 9^\circ$ the mean value of P_{23} is almost zero. One also observes how the sample standard deviation changes as θ_{13} varies and sees that it is maximal at $\sigma_{23} = 0.28$ for the range $0.1^\circ \lesssim \theta_{13} \lesssim 1^\circ$ and almost zero when $\theta_{13} \sim 9^\circ$. This figure shows how the measurement of θ_{13} has brought clarity to the issue of turbulence and supernova neutrinos. For θ_{13} outside the range $0.1^\circ \lesssim \theta_{13} \lesssim 1^\circ$ the distribution of P_{23} is essentially a delta function at either zero or unity; for θ_{13} inside the range $0.1^\circ \lesssim \theta_{13} \lesssim 1^\circ$ the distribution is uniform. Thus when θ_{13} was unknown it was impossible to determine whether the effect of small amplitude turbulence was negligible or overwhelming. The measurement of a large value of θ_{13} indicates it is the former and the result has consequences for the observability of spectral features in the next Galactic supernova burst signal.

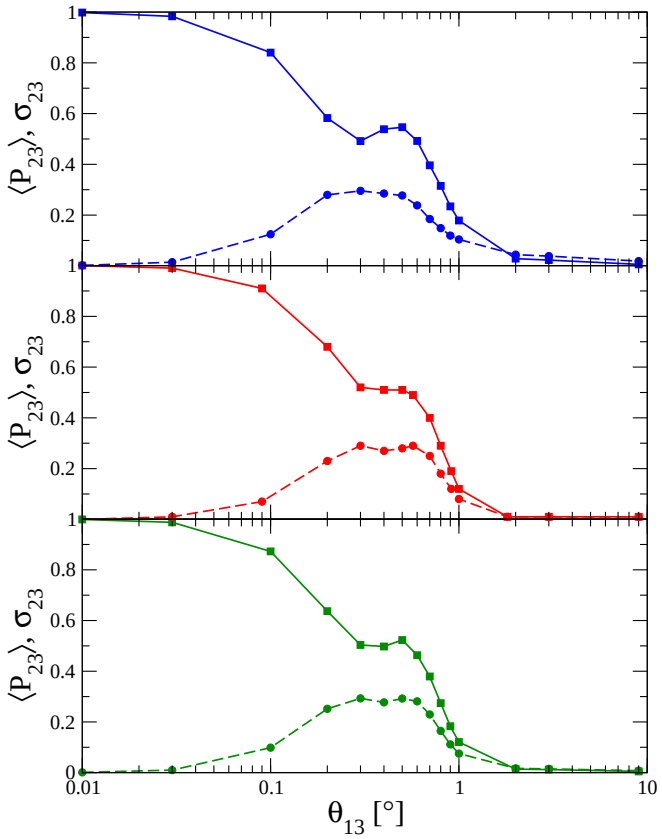

FIG. 5. The mean of the transition probability, $\langle P_{23}\rangle$ (solid line, squares) and the standard deviation σ_{23} (dashed line, circles) as function of the mixing angle θ_{13}. The turbulence amplitude is set to $C_\star = 1\%$ and $\{N_k, N_d\} = \{50, 5\}$. In the top panel the neutrino energy is 20 MeV, in the middle it is 25 MeV, and in the bottom it is 30 MeV.

B. Large Amplitudes

1. *The neutrino mixing channels*

For large amplitudes, $C_\star \gtrsim 0.1$, the effects of turbulence are no longer restricted to the H resonance channel but appear in numerous places. The first effect worth noting is that the distribution of the H resonance channel transition probability, P_{23} in the case of a normal hierarchy, becomes independent of θ_{13}. This can be seen in figure (6) where the reader will observe the evolution of the mean value of this transition probability $\langle P_{23}\rangle$ as a function of $C_\star$. For the two values of θ_{13} considered, the spread in $\langle P_{23}\rangle$ at small amplitudes has disappeared by $C_\star \sim 0.3$. We also notice that around this same turbulence amplitude there begins the shift to three-flavor depolarization where $\langle P_{23}\rangle = 1/3$.

In addition to the changes in the H resonance channel we also begin to observe mixing in the low (L) density resonance channel, between ν_1 and ν_2 as the amplitude grows. This simultaneous mixing between ν_1 and ν_2 and ν_2 and ν_3 breaks HL factorization and Kneller & Volpe presented two examples which explicitly showed broken HL factorization. For the neutrino mixing parameters we are using, the ratio of H and L resonance densities (using the two-flavor formula) is $\rho_H/\rho_L = (\delta m^2_{23}\cos 2\theta_{13})/(\delta m^2_{12}\cos 2\theta_{12}) \approx 90$. This large ratio would seem to imply that we need fluctuations of order $F \sim 1$ because only if $F = -0.99$ would the density fluctuation give $\rho_H(1+F) \approx \rho_L$. Three effects soften this requirement: the L resonance has a large width - $\Delta\rho_L/\rho_L = \tan 2\theta_{12} \sim 1$, the density in the turbulence region can be much lower than the resonance density ρ_H for the given neutrino energy - see figure (1), and, finally, our choice of a Gaussian random field for the turbulence will ensure that large fluctuations will occur occasionally no matter what we use for the amplitude, larger amplitudes just make the extremal fluctuations more probable. The clearest signature of broken HL factorization is a non-zero transition probability P_{31} because only if HL factorization is broken can we generate an effective mixing between ν_1 and ν_3. To see this we consider the S-matrices for the case of factored HL resonances and

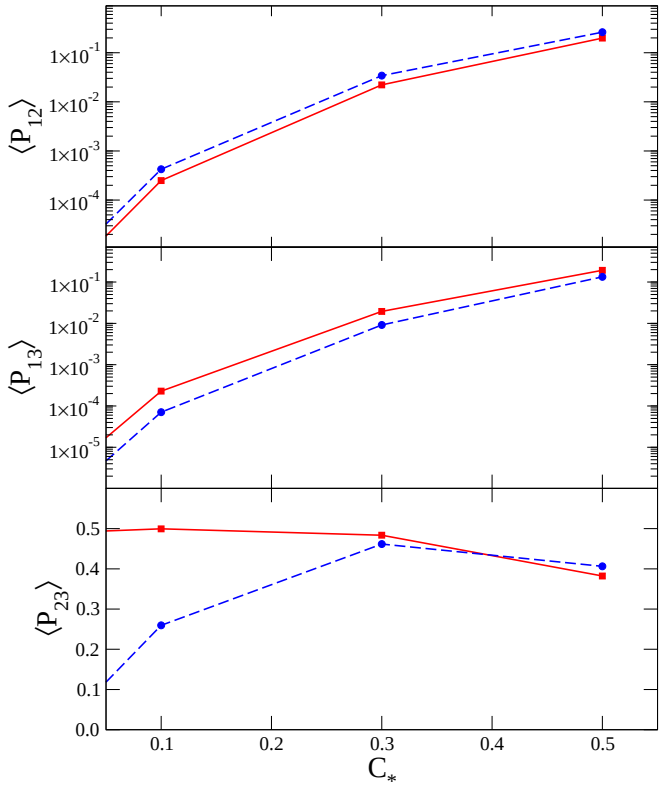

FIG. 6. The mean of the transition probabilities P_{12} - top panel - P_{13} - center panel - and P_{23} - bottom panel - through anisotropic turbulence as a function of $C_\star$ for antineutrinos emitted from a single point. Each curve corresponds to a different value of θ_{13}: $\sin^2 2\theta_{13} = 4 \times 10^{-4}$ are squares joined by solid lines, $\sin^2 2\theta_{13} = 0.1$ are circles joined by dashed lines. The neutrino energy is 25 MeV.

broken factorization. The S-matrix for passing through one or several H resonances, S_H, has the general form

$$S_H = \begin{pmatrix} 1 & 0 & 0 \\ 0 & \alpha_H & \beta_H \\ 0 & -\beta_H^\star & \alpha_H^\star \end{pmatrix} \tag{6}$$

where α_H and β_H are Cayley-Klein parameters. Similarly the S-matrix for L resonances, S_L, is

$$S_L = \begin{pmatrix} \alpha_L & \beta_L & 0 \\ -\beta_L^\star & \alpha_L^\star & 0 \\ 0 & 0 & 1 \end{pmatrix} \tag{7}$$

where α_H and β_H are Cayley-Klein parameters for the L resonance. If HL factorization holds then the S-matrix which describes the evolution for the neutrino through the entire profile is $S = S_L S_H$. If all the L resonances occur after the H resonances then we find the transition probability $P_{31} = |S_{31}|^2$ is identically zero. But if additional H and L resonances occur, denoted by S'_H and S'_L, then the S-matrix describing the neutrino evolution is of the form $S = S'_L S'_H S_L S_H$ and $P_{31} = |\beta'_H|^2 |\beta_L|^2$ will be non-zero. In figure (7) we show frequency distributions

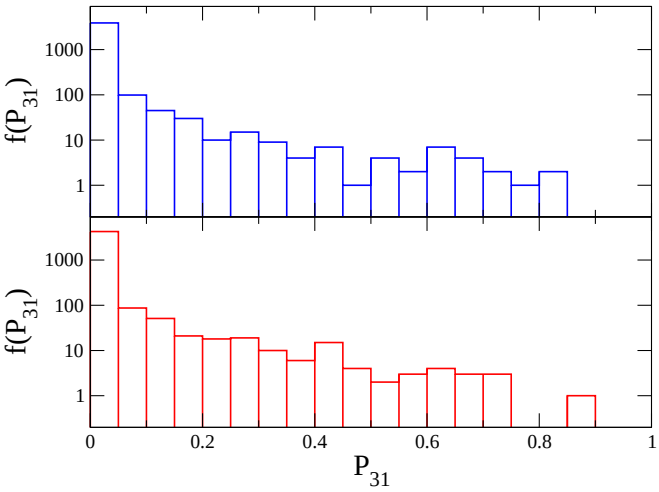

FIG. 7. The frequency distribution of the transition probability P_{31} for a turbulence amplitude is set to $C_\star = 0.3$. The neutrino energy is 25 MeV and we used $N_k = 50$, $N_d = 5$ for the turbulence generator. The top panel used a value of θ_{13} given by $\sin^2 2\theta_{13} = 0.1$ and the bottom panel is for $\sin^2 2\theta_{13} = 4 \times 10^{-4}$.

of the transition probability P_{31} for neutrinos at two values of θ_{13} when $C_\star = 0.3$. The distributions are clearly non-zero for non-zero P_{31} as expected if HL factorization were broken. The distributions fall rapidly as something like inverse-power laws, $f(P_{31}) \propto 1/P_{31}^n$ with $n \sim 2$ or exponentials for this particular calculation.

Other mixing channels which were previously delta-distributed for small turbulence amplitudes - such as P_{12} and P_{13} - also begin to possess similar inverse power-law/exponential distributions when $C_\star \gtrsim 0.1$ and their means increase quadratically with $C_\star$. The evolution of these two transition probabilities is also shown in figure (6). The figure shows that $\langle P_{12} \rangle$ at some fixed $C_\star$ increases as θ_{13} increases but $\langle P_{13} \rangle$ decreases as θ_{13} increases though, in both cases, the change is not very large. The anticorrelation between $\langle P_{12} \rangle$ and $\langle P_{13} \rangle$ is a reflection of the unitarity requirement that $\Sigma_j P_{ij} = 1$ for a given i.

2. *The antineutrino mixing channels*

In addition to breaking HL factorization, large amplitude turbulence induces effects in the *non-resonance* channels particularly $\bar{\nu}_1 \leftrightarrow \bar{\nu}_2$ regardless of the hierarchy, $\bar{\nu}_1 \leftrightarrow \bar{\nu}_3$ for a normal hierarchy and P_{23} for an inverted hierarchy. If we stick with considering the normal hierarchy case then we can compute the mean of the non-resonant transition probabilities $\bar{P}_{12}$, $\bar{P}_{13}$ and $\bar{P}_{23}$ as a function of the mixing angle θ_{13} and turbulence amplitude $C_\star$. These are shown in figure (8). Like $\langle P_{12} \rangle$ and $\langle P_{13} \rangle$ shown in figure (6), the reader will observe that the three transition probabilities grow rapidly with $C_\star$ reaching the levels of $\langle \bar{P}_{12} \rangle \sim (10\%)$, $\langle \bar{P}_{13} \rangle \sim (1\%)$ and $\langle \bar{P}_{23} \rangle \sim (1\%)$

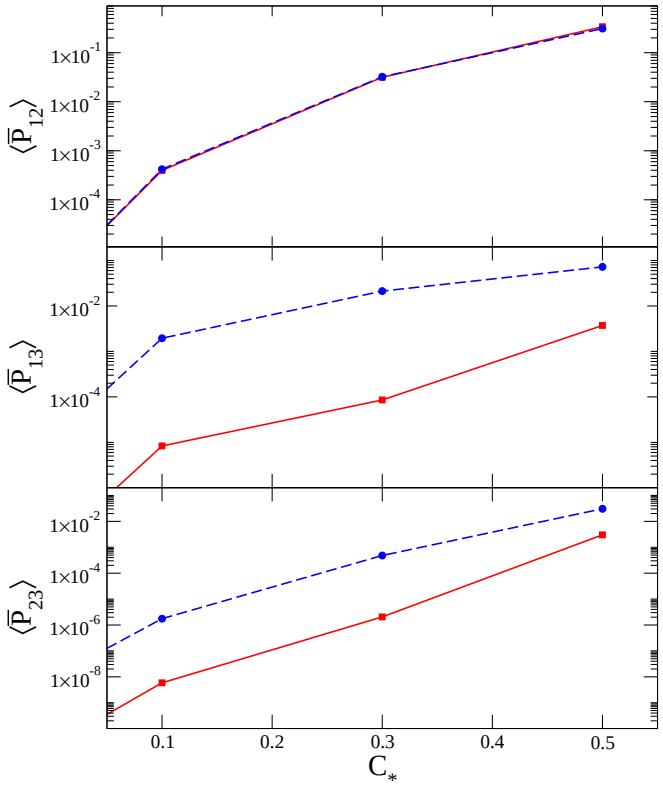

FIG. 8. The mean of the transition probability $\bar{P}_{12}$ - top panel - $\bar{P}_{13}$ - center panel - and $\bar{P}_{23}$ - bottom panel - as a function of $C_\star$ for antineutrinos. Each curve corresponds to a different value of θ_{13}: $\sin^2 2\theta_{13} = 4 \times 10^{-4}$ are squares and $\sin^2 2\theta_{13} = 0.1$ are circles.

at $C_\star \sim 0.5$. Further comparison with figure (6) reveals $\langle P_{12} \rangle \approx \langle \bar{P}_{12} \rangle$ and the expectation values for the transition probabilities $\bar{P}_{13}$ and $\bar{P}_{23}$ are both smaller than $\langle P_{13} \rangle$ by roughly an order of magnitude and much more sensitive to θ_{13}. The expectation value for P_{13} varied by a factor of ~ 2 when θ_{13} allowed to float, here $\bar{P}_{13}$ and $\bar{P}_{23}$ change by an $\sim 1-2$ orders of magnitude when increasing from $\sin^2 2\theta_{13} = 4 \times 10^{-4}$ to $\sin^2 2\theta_{13} = 0.1$. This same sensitivity to θ_{13} was explained in Kneller & Volpe as due to the proportionality of the antineutrino diabaticity parameter $\bar{\Gamma}_{13}$ to the vacuum mixing angle. The current preference for θ_{13} close to $\theta_{13} \sim 9^\circ$ indicates $\langle \bar{P}_{13} \rangle$ and $\langle \bar{P}_{23} \rangle$ can be of order a few percent if $C_\star \sim 0.5$.

IV. SUMMARY AND CONCLUSIONS

The effects of supernova turbulence upon the flavor composition of neutrinos that pass through it depend upon the numerous parameters that one needs to introduce. Using a supernova density profile taken from a simulation 4.5 s post-bounce, turbulence of amplitude $C_\star = 1\%$ only affects the H resonance mixing channel to any appreciable degree and then only for mixing angles in the range $0.1^\circ \lesssim \theta_{13} \lesssim 1^\circ$. Now that we know θ_{13} is closer to 9° we can be definitive and state there is little effect of small amplitude density fluctuations. This result is valid for a range of neutrino energies - all those which have MSW resonances in the region where the turbulence is located. The removal of turbulence effects upon the neutrinos for small amplitudes has important consequences for the prospect of observing signatures of collective and shock wave effects in supernova neutrino burst signals, which is explored in Lund & Kneller [57].

For the same post-bounce epoch, the turbulence effects metastasize as the amplitude increases. The sensitivity to θ_{13} in the H resonant mixing channel is lost and this transistion probability reaches the depolariation limit. For large amplitudes HL factorization becomes increasingly broken. For amplitudes of $C_\star \gtrsim 0.3$, and a normal hierarchy the expectation values of the transition probabilities P_{12} - the L resonance channel - P_{13}, P_{23} and $\bar{P}_{12}$ are of order 10% or greater; in an inverted hierarchy it is the transition probabilities P_{12}, $\bar{P}_{12}$, $\bar{P}_{13}$ and $\bar{P}_{23}$ whose expectation values are of equivalent magnitudes. None appear to be sensitive to θ_{13} and these channels are the most promising for observing the signatures of large amplitude turbulence. The remaining mixing channels for each hierarchy, $\bar{P}_{13}$ and $\bar{P}_{23}$ for a normal case, P_{13}, P_{23} and $\bar{P}_{23}$ for an inverted, are small, a few percent, even at $C_\star \sim 0.5$ but we find large θ_{13} increases their sensitivity to turbulence. Further discussions of the effects of turbulence at large amplitudes when combined with collective and shock wave effects can be found in Lund & Kneller [57].

ACKNOWLEDGMENTS

This work was supported by DOE grant DE-SC0006417, the Topical Collaboration in Nuclear Science "Neutrinos and Nucleosynthesis in Hot and Dense Matter", DOE grant number DE-SC0004786, and an Undergraduate Research Grant from NC State University.

[1] J. T. Pantaleone, Phys. Lett. B, **287**, 128 (1992).
[2] S. Samuel, Phys. Rev. D, **48**, 1462 (1993).
[3] H. Duan, G. M. Fuller and Y. Z. Qian, Phys. Rev. D**74**, 123004 (2006)
[4] S. Pastor, G. G. Raffelt and D. V. Semikoz, Phys. Rev. D**65**, 053011 (2002)
[5] S. Hannestad, G. G. Raffelt, G. Sigl and Y. Y. Y. Wong, Phys. Rev. D**74**, 105010 (2006) [Erratum-ibid. D **76**, 029901 (2007)]

[6] H. Duan, G. M. Fuller, J. Carlson and Y. Z. Qian, Phys. Rev. D**74** 105014 (2006)
[7] G. G. Raffelt and A. Y. Smirnov, Phys. Rev. D**76**, 081301 (2007) [Erratum-ibid. D **77**, 029903 (2008)]
[8] Raffelt, G. G., Phys. Rev. D**78** 125015 (2008)
[9] Duan, H., & Friedland, A., Phys. Rev. Lett., **106** 091101 (2011)
[10] Reid, G., Adams, J., & Seunarine, S., Phys. Rev. D**84** 085023 (2011)
[11] Chakraborty, S., Fischer, T., Mirizzi, A., Saviano, N., & Tomàs, R., Phys. Rev. Lett.**107** 151101 (2011)
[12] Galais, S., Kneller, J., & Volpe, C., Journal of Physics G Nuclear Physics, **39** 035201 (2012)
[13] Cherry, J. F., Carlson, J., Friedland, A., Fuller, G. M., & Vlasenko, A., Phys. Rev. Lett.**108** 261104 (2012)
[14] Sarikas, S., Tamborra, I., Raffelt, G., Hüdepohl, L., & Janka, H.-T., Phys. Rev. D**85** 113007 (2012)
[15] Mirizzi, A., & Serpico, P. D., Phys. Rev. Lett.**108** 231102 (2012)
[16] H. Duan, G. M. Fuller and Y. Z. Qian, arXiv:1001.2799 [hep-ph].
[17] H. Duan and J. P. Kneller, J. Phys. G **36**, 113201 (2009) [arXiv:0904.0974 [astro-ph.HE]].
[18] S. P. Mikheev and A. I. Smirnov, Nuovo Cimento C **9** 17 (1986)
[19] L. Wolfenstein, Phys. Rev. D**17** 2369 (1978)
[20] R. C. Schirato and G. M. Fuller, arXiv:astro-ph/0205390.
[21] K. Takahashi, K. Sato, H. E. Dalhed and J. R. Wilson, Astropart. Phys. **20** 189 (2003)
[22] G. L. Fogli, E. Lisi, D. Montanino and A. Mirizzi, Phys. Rev. D**68** 033005 (2003)
[23] R. Tomas, M. Kachelriess, G. Raffelt, A. Dighe, H. T. Janka and L. Scheck, JCAP **0409** 015 (2004)
[24] S. Choubey, N. P. Harries and G. G. Ross, Phys. Rev. D**74** 053010 (2006)
[25] J. P. Kneller, G. C. McLaughlin and J. Brockman, Phys. Rev. D**77** 045023 (2008)
[26] J. Gava, J. Kneller, C. Volpe and G. C. McLaughlin, Phys. Rev. Lett.**103** 071101 (2009)
[27] Borriello, E., Chakraborty, S., Mirizzi, A., Serpico, P. D., & Tamborra, I., Phys. Rev. D**86** 083004 (2012)
[28] Lunardini, C., Müller, B., & Janka, H.-T., Phys. Rev. D**78** 023016 (2008)
[29] Duan, H., Fuller, G. M., Carlson, J., & Qian, Y.-Z., Phys. Rev. Lett.**100** 021101 (2008)
[30] Cherry, J. F., Fuller, G. M., Carlson, J., Duan, H., & Qian, Y.-Z., Phys. Rev. D**82** 085025 (2010)
[31] Kitaura, F. S., Janka, H.-T., & Hillebrandt, W., Astron. and Astrophys. **450** 345 (2006)
[32] Dessart, L., Burrows, A., Ott, C. D., et al., Astrophys. J.**644** 1063 (2006)
[33] Fischer, T., Whitehouse, S. C., Mezzacappa, A., Thielemann, F.-K., & Liebendörfer, M., Astron. and Astrophys. **517** A80 (2010)
[34] Abe, K., Abgrall, N., Ajima, Y., et al., Phys. Rev. Lett.**107** 041801 (2011)
[35] Ahn, J. K., Chebotaryov, S., Choi, J. H., et al., Phys. Rev. Lett.**108** 191802 (2012)
[36] An, F. P., Bai, J. Z., Balantekin, A. B., et al., Phys. Rev. Lett.**108** 171803 (2012)
[37] Abe, Y., Aberle, C., Akiri, T., et al., Phys. Rev. Lett.**108** 131801 (2012)
[38] A. S. Dighe and A. Yu. Smirnov, Phys. Rev. D**62** 033007 (2000)
[39] Z. Maki M. Nakagawa and S. Sakata, Prog. Theor. Phys., **28** 870 (1962)
[40] K. Nakamura *et al.* [Particle Data Group Collaboration], J. Phys. G **G37**, 075021 (2010).
[41] Murphy, J. W., & Meakin, C., Astrophys. J.**742** 74 (2011)
[42] Dolence, J. C., Burrows, A., Murphy, J. W., & Nordhaus, J., arXiv:1210.5241 (2012)
[43] Ott, C. D., Abdikamalov, E., Moesta, P., et al., arXiv:1210.6674 (2012)
[44] Hanke, F., Marek, A., Müller, B., & Janka, H.-T., Astrophys. J.**755** 138 (2012)
[45] Pejcha, O., & Thompson, T. A., Astrophys. J.**746** 106 (2012)
[46] Müller, B., Janka, H.-T., & Heger, A., Astrophys. J.**761** 72 (2012)
[47] Takiwaki, T., Kotake, K., & Suwa, Y., Astrophys. J.**749** 98 (2012)
[48] Lentz, E. J., Bruenn, S. W., Harris, J. A., et al., arXiv:1301.1326 (2013)
[49] Loreti, F. N. and Qian, Y.-Z. and Fuller, G. M. and Balantekin, A. B., Phys. Rev. D**52** 6664 (1995)
[50] G. Fogli, E. Lisi, A. Mirizzi and D. Montanino, JCAP **0606** 012 (2006) [arXiv:hep-ph/0603033]
[51] A. Friedland and A. Gruzinov, arXiv:astro-ph/0607244
[52] Kneller, J. and Volpe, C.,Phys. Rev. D**82** 123004 (2010)
[53] J. P. Kneller and G. C. McLaughlin, Phys. Rev. D**73** 056003 (2006)
[54] Dasgupta, B., and Dighe, A., Phys. Rev. D**75** (2007) 093002
[55] Kneller, J. P., and McLaughlin, G. C., Phys. Rev. D**80** 053002 (2009)
[56] Galais, S., Kneller, J., Volpe, C., & Gava, J., Phys. Rev. D**81** 053002 (2010)
[57] Lund, T., & Kneller, J. P. 2013, arXiv:1304.6372
[58] J. P. Kneller, arXiv:1004.1288 [hep-ph].
[59] Kramer, P. R., Kurbanmuradov, O., & Sabelfeld, K. Journal of Computational Physics **226** 897 (2007)
[60] Kneller, J. P., McLaughlin, G. C., & Patton, K. M. 2012, arXiv:1202.0776